Journal of Power Sources 198 (2012) 351–358

Contents lists available at SciVerse ScienceDirect

Journal of Power Sources

journal homepage: www.elsevier.com/locate/jpowsour

Monitoring dynamic thermal behavior of the carbon anode in a lithium-ion cell using a four-probe technique

Rengaswamy Srinivasan*

Applied Physics Laboratory, The Johns Hopkins University, Laurel, MD 20723-6099, United States

ARTICLE INFO

Article history:
Received 8 August 2011
Received in revised form
23 September 2011
Accepted 24 September 2011
Available online 1 October 2011

Keywords:
Lithium battery
Internal temperature monitor
Phase meter
SEI layer
Entropy

ABSTRACT

We describe a four-probe electrical technique that enables real-time temperature monitoring of the carbon anode in a 53 Ah lithium-ion rechargeable cell during charging and discharging. This technique uses only electrical contacts to the positive and negative terminals of the cell, eliminating the need to insert temperature sensors inside the cell. Our method is based on the intrinsic relationship of anode temperature with phase shift between an applied sinusoidal current and the resulting voltage, valid within the 5% and 95% range of the state-of-charge (SoC) of the cell. Using this technique, we demonstrate that the anode temperature (T_{anode}) can deviate from the temperature measured at the outside surface (T_{surf}) of the cell during charge and discharge. Additionally, we show that anode temperature is primarily determined by entropy change at the anode or by resistive impedance of the anode, depending on the environment temperature (T_{env}).

1. Introduction

Excursions in the anode temperature (T_{anode}) relate to the stability of the solid-electrolyte-interphase (SEI) layer, as well as adverse events such as venting and rupture [1,2]. Excursions in the internal temperature can occur rapidly, within seconds to tens of seconds [3]. Typically, conventional surface-mounted temperature sensors exhibit response profiles that are too slow to sense the temperature spikes occurring within the cell, therefore unsuitable to guard against venting and rupture. Today, however, placing thermal sensors at the outside surface remains the only practical means of monitoring the internal temperature [4,5]. New and convenient approaches are needed to support real-time continuous monitoring the temperature within a cell to ensure safety and longevity.

Heat can destroy a lithium cell with modest but rapid elevations in temperature. Conjectural evidence relates elevated cell temperatures to damage in the SEI layer, electrolyte degradation and cathode decomposition. These processes are heat-induced, but they are also exothermic, resulting in an auto-catalytic process known as thermal runaway [6]. Prior studies indicate that the nominally protective SEI layer can be damaged at temperatures as low as 100 °C [1,2,7]. Moreover, the time scale associated with thermal runaway is short, depending on the cell's state of charge (SoC). At 100% SoC, thermal runaway occurs within a few seconds, whereas at less than 50% SoC, this process may require tens of seconds (with ambient temperature 25 °C) [3]. Existing surface-mounted temperature sensors are inadequate to track internal temperature changes, regardless of the sampling rate used to digitize sensor output. This is because surface mounted temperature is a low-pass-filtered reflection of internal temperature. This means that fast changes in internal temperature (occurring on the order of less than a few seconds) are not reflected in surface-mounted temperature. As a result, surface-mounted temperature are inadequate to detect or predict thermal runaway.

Recently, we developed a technique that is capable of estimating internal temperature in lithium-ion cells with components that are completely external to the cell, called battery internal temperature sensor (BITS) [8,9]. This technique uses phase shift (ϕ) in the impedance of the cell evaluated at 40 Hz to estimate T_{anode}. This is in contrast to conventional impedance techniques that require multiple frequencies with model fitting [10,11]. In this article, we demonstrate that BITS reliably and rapidly tracks dynamic changes in the anode temperature of a 53-Ah cell under charge and discharge across various environment temperatures. As a measure of accuracy, temperature at the anode derived from BITS is compared against the temperature change predicted by: (i) entropy data for carbon anode from the literature; and (ii) impedance exerted by the anode against the flow of the current during change and discharge.

* Corresponding author. Tel.: +1 443 778 6378; fax: +1 443 778 5937.
E-mail addresses: Rengaswamy.srinivasan@jhuapl.edu, srinir@comcast.net, srinir1@jhuapl.edu

0378-7753/$ – see front matter © 2011 Elsevier B.V. All rights reserved.
doi:10.1016/j.jpowsour.2011.09.077

Nomenclature

BITS	battery internal temperature sensor
C	capacity of a cell in units of Ah
i	current; sign is negative for discharge
R_a	resistive impedance of the anode in a rechargeable Li-ion cell; it is a temperature-dependent parameter
i^2R_a	resistive heating in units of Watt (W)
SoC	state of charge
SEI	solid electrolyte interphase
T	temperature (K or °C)
T_{anode}	temperature of the anode
T_{env}	temperature surrounding the outer surface of the cell, typically the temperature of the environmental chamber
T_{surf}	temperature at the outer surface of the cell measured by a K-type thermocouple mounted on the middle of the broad side of the outer metal casing of the cell

Greek letters

ϕ	phase shift between an applied sinusoidal current and the resulting voltage
ΔS	change in entropy
$\Delta S'$	change in entropy due to a specific amount of mole equivalent of Li^+
τ	time (s)
τ'	a specific amount of time associated with discharge
$T\Delta S$	energy associated with change in entropy ($J\,mol^{-1}\,K^{-1}$)
$T\Delta S'$	$T\Delta S$ for a specific number of moles ($J\,K^{-1}$)
$T\Delta S'/\tau'$	average power released by $T\Delta S'$ over τ' (W)

2. Methods

Impedance technique that is often referred to as electrochemical impedance spectroscopy or EIS was used to characterize a lithium-ion (Li-ion) rechargeable cell. We implemented the impedance technique in two different ways: (i) for T_{anode} measurements (BITS), we used a 40 Hz sinusoidal current signal and recorded only the phase shift; and (ii) for estimating the anode impedance, we used sinusoidal current signals at multiple frequencies, generally in the 10–1000 Hz range, and recorded the real and imaginary components. More details about the impedance approach is described below.

2.1. BITS-based phase measurement

The BITS technique uses the phase shift component of the cell impedance at 40 Hz as a measure of temperature at the anode. Previous work has shown that impedance due to the SEI layer is almost fully dependent upon the temperature of the cell [10–12], and virtually independent of the state-of-charge (SoC) of the cell. At frequencies greater than 30 Hz, impedance of the SEI layer is approximately equal to measured impedance of the cell, because anode impedance dominates cell impedance in this domain.

We previously demonstrated BITS in three different cell models (2.3 Ah, 4.4 Ah and 53 Ah), showing that phase shift at any frequency in the 40–100 Hz range produces a reasonable estimate of T_{anode} [8]. This eliminates the need for multiple frequency measurements in temperature monitoring suggested by other techniques [10–12]. Our previous work also demonstrated that phase shift is independent of SoC when SoC is within 5–95% of maximum charge [8].

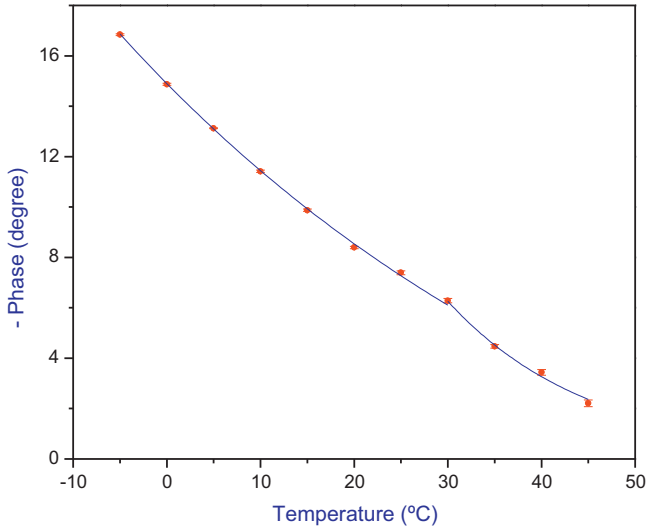

Fig. 1. Variation of phase shift, ϕ, with the environmental temperature of a 53-Ah GS Yuasa LSE50-002 Li-ion rechargeable cell. The solid lines are fitted curves (exponential decay) to the ϕ versus temperature data. The fitting showing two separate exponential behavior was used as "calibration" to infer internal temperature (T_{anode}) by monitoring ϕ online during charge and discharge of the cell.

To apply BITS to the cell used in this study, we first measured the relationship between 40 Hz phase shift and T_{anode} while keeping the cell at 50% SoC and open circuited. The $-\phi$ versus temperature data are shown in Fig. 1; the break around 30 °C is associated with the thickening of the SEI layer due to the chemical reaction between the carbon anode and electrolyte [8]. Subsequently, we measured 40 Hz phase shift continuously during charge and discharge. Instantaneous estimates of T_{anode} were generated by using Fig. 1 as a look-up table. The accuracy of this approach relied on the invariance of phase shift to SoC, as previously demonstrated [8].

The BITS-based phase shift measurements were made on a 53-Ah GS Yuasa LSE50-002 cell under the dynamic condition of charge and discharge at different environmental temperatures in the 0–45 °C range. During the measurements, the cell was housed inside a Thermotron Model S-1.2 chamber to maintain the temperature of the environment around the cell. Arbin Instruments Model BT2000 was used for charging and discharging the cell, and to monitor the cell's surface temperature through a K-type thermocouple mounted on the middle of the broad side of the outer metal casing of the cell. Solartron Electrochemical Interface (potentiostat/galvanostat) Model SI 1287, and Frequency Response Analyzer Model SI 1250 were used for measuring the phase shift.

2.2. Anode impedance measurement

The impedance of the cell was measured under static condition (cell not under charge or discharge) at different temperatures in the −10 °C to 50 °C range, and at different states-of-charge at each temperature in the 5–95% range. The frequency range for the impedance measurement was 0.8–1000 Hz, sampled at 20 frequencies per decade, and the amplitude of the perturbation current was 200-mA rms. The impedance data were used to compute the resistive impedance of the anode at various temperatures within the −10 °C to 50 °C range.

2.3. Specifications for the Li-ion cell

The 53-Ah GS Yuasa LSE50-002 cell is a prismatic, 1.5-kg model containing graphite anodes and $LiCoO_2$ cathodes packed as a layered Swiss-jelly roll. The cell contains an equivalent of

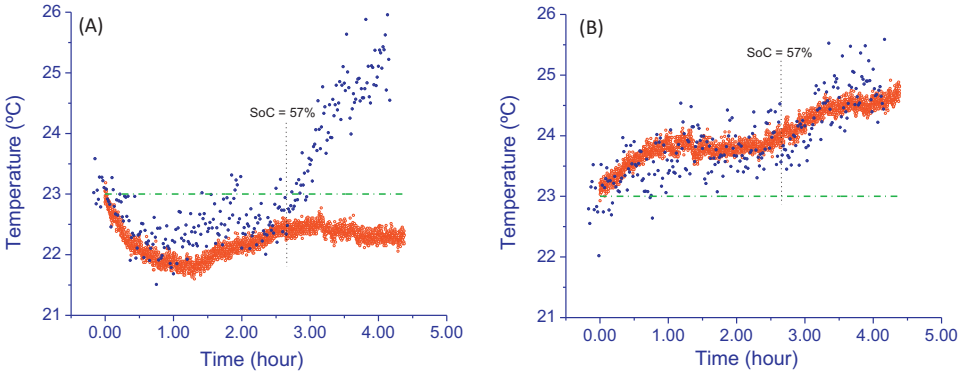

Fig. 2. Anode temperature, T_{anode} (blue), and surface temperature, T_{surf} (red) behavior of the GS Yuasa cell in a 23 °C environment under: (A) $C/5$ charge; and (B) $C/5$ discharge. Before charge and discharge, the cell was at rest for 18 h, allowing its internal temperature to equilibrate with the temperature of the environment, T_{env}. In this, and in Figs. 3–7, the dotted green line represents the T_{env}. (For interpretation of the references to color in this figure legend, the reader is referred to the web version of the article.)

15 g (2.16 mol) of lithium; in a fully charged state, roughly 50% (1.08 mol) of lithium is assumed to be present in the carbon anode. The cell had been previously used under widely varying temperature and load conditions, charged and discharged (full depth) for about forty cycles including one instance of a high-rate discharge at 1600-A from full charge to complete discharge. If discharged at $C/2$-rate or less at room temperature (23 °C), the cell yielded 50-Ah and 196-Wh capacities; the C in $C/2$ refers to the capacity of the cell in units of ampere-hour (Ah).

2.4. Dynamic temperature monitoring

T_{anode} was monitored (through the BITS-based ϕ measurement) under three sets of dynamic conditions. The term "dynamic" refers to the cell being under continuous charge or discharge during the T_{anode} measurements.

In Set 1, the cell was in a 23 °C environment (T_{env} = 23 °C) and was charged or discharged at $C/5$ rate (10-A rate) in constant current mode. The following precaution was taken to ensure that at the beginning of the dynamic measurement of T_{anode}, the cell's internal temperature was in equilibrium with T_{env}: a fully discharged cell was first charged to 5% SoC, allowed to rest for 18 h with no charge or discharge current flow. After the 18 h at rest, while monitoring T_{anode}, the cell was charged to 90% of its capacity. Similarly, a fully charged cell was discharged first to 95% SoC, left to equilibrate with T_{env} for 18 h, and then while monitoring T_{anode}, discharged to 5% SoC. The 18 h at rest T_{env} was assumed to bring the cell's internal temperature to be the same as T_{env}.

Set 2 measurements were almost similar to the Set 1, except the cell was first discharged at 5-A rate to full depth-of-discharge, and immediately recharged at 10-A rate, all under constant current mode; unlike in Set 1, the cell was not allowed a rest period with zero current flow. In the absence of rest after discharge and charging, the cell's internal temperature would not have fully equilibrated with the T_{env}, representing the most common battery charging procedure.

In Set 3, the cell was discharged at rates that were typically >$C/5$, and at four different T_{env}: 0, 23, 38 and 45 °C. Before discharge at each T_{env}, the cell was always charged at $C/5$ rate at 23 °C to 90% of its capacity, rested for 18 h, followed by discharge using a current profile sequence of −5 A for 2 h; −25 A for 0.4 h; −45 A for 0.22 h; −10 A for 1 h; and −5 A for the remainder of duration until the cell was discharged to 5% SoC. In this profile, each of the first four steps (−5, −25, −45 and −10-A) constituted an equivalent of 10-Ah capacity of the cell. The profile-based discharges were repeated at 0, 23, 38 and 45 °C.

3. Results and discussion

The results from the dynamic monitoring of the anode temperature, T_{anode} in the 53-Ah cell under charge and discharge at various temperatures are presented next. The data below demonstrate that BITS, which is a single-frequency phase shift technique to monitor T_{anode}, originally developed for cells in open loop [8,9] is applicable to cells during charge and discharge. The T_{anode} data obtained under dynamic conditions viewed in conjunction with the anode's resistive impedance data shed light on the entropy-related behavior of anode.

3.1. Set 1, charging and discharging in a 23 °C environment after equilibration with T_{env}

The phase shift, ϕ values were converted into T_{anode} using the data in Fig. 1 as the look-up table; the results, along with the respective T_{surf} and T_{env} versus time are shown in Fig. 2A and B. The green dot-dash line in the figures represents the temperature of the cell's surroundings, T_{env}, i.e., the temperature of the space inside the environmental chamber. The T_{anode} and T_{surf}, are represented by the blue and red dots, respectively.

During charging, the T_{surf} was always lower than the T_{env} (23 °C). During the early part of the discharge, the T_{surf} dropped by about 1.5 °C below T_{env}, the lowest point over the entire time of charge. On the other hand, the T_{anode} that registered initially a similar decrease, started increasing when the cell reached 57% SoC; the increasing trend of the T_{anode} continued until the SoC reached 90%. The initial drop in the surface temperature is consistent with the earlier observations by other research groups; however, the persistence of the T_{surf} remaining below the T_{env} is inconsistent with the earlier reports. The inconsistency appears to be caused by the initial thermal state of the cell, namely, forcing the cell's internal temperature to settle at T_{env} through the 18-h equilibration process. (Charging the cell immediately after it is discharged, without allowing its internal temperature to equilibrate with T_{env}, does generate T_{surf} values that are consistent with the earlier report, and will be discussed in Section 3.2; Fig. 3.)

The drop in the T_{surf} during the charging is generally attributed to a net positive change in entropy (+ΔS) within the cell, due to the removal of Li^+ ions from the cathode. However, on the anode side, during charging, the change in the entropy is known to be negative (−ΔS), and it should cause the anode temperature to increase. In Fig. 2A, the T_{anode} indeed shows a marked increase, especially when SoC ≥57%. Note that the sudden jump in T_{anode}, when the SoC reaches 57%, matches with the transition of the anode from Stage II (anode composition: LiC_{12}) to Stage I (anode composition: LiC_6)

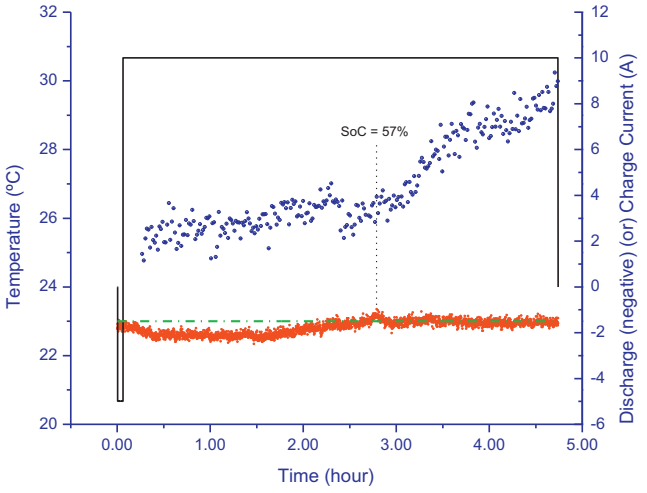

Fig. 3. Anode temperature, T_{anode} (blue), and surface temperature, T_{surf} (red) behavior of the GS Yuasa cell in a 23 °C environment under $C/5$ charge. Unlike the condition in Fig. 2A, the cell was not rested before charging; a discharge happened immediately prior to the charging. The discharging and charging currents are shown in solid black line, referenced to the Y-axis scale on the right. (For interpretation of the references to color in this figure legend, the reader is referred to the web version of the article.)

[13]. Incidentally, the transition from Stage II to Stage I (LiC_{12} to LiC_6) is associated with a step change in the entropy of the anode, which is also reported in earlier works [14,15].

In addition, the signs of the slopes of the T_{surf} versus time and the T_{anode} versus time curves provide clues to the dominance of the cathode over the anode in its contribution to the thermal behavior of the cell. Previous thermodynamic models and tests on anode and cathode half cells have shown that the magnitude of ΔS for the cathode is larger than that of the anode [5]. Therefore one would expect the cell temperature to be influenced by the heat changes in the cathode more than the heat changes in the anode. Thus, while charging at $C/5$ rate, the large positive change in the ΔS of the cathode should cool the cell more than the relatively smaller negative change in the ΔS of the anode that heats the cell. The observed trend in the T_{surf} shown in Fig. 2A indicating cooling of the cell, while the anode is heating up, provides an indirect evidence to the dominance of entropy change in the cathode over that of the anode. Conversely, although the T_{surf} is influenced by the cooling of the cathode and registers a temperature that is a few degrees below the 23 °C environment, the data in Fig. 2A showing $T_{anode} > T_{surf}$ is consistent with the exothermic thermodynamic process, namely negative change in ΔS.

Next, during the discharge of a thermally equilibrated cell from 90% to 5% SoC, the T_{surf} showed an increase from the beginning, always remaining above the T_{env} (Fig. 2B). Unlike during charging, the difference in the temperature between the T_{surf} and T_{anode} was little ($T_{anode} \approx T_{surf}$). Furthermore, during discharging, when the SoC reached 57%, there was a step-increase in T_{anode}, similar to the step-increase in T_{anode} during charging (Fig. 2A); only during discharging, the step-increase was also observed in the T_{surf}. It appears that the Stage I–Stage II transition causes a step-change in the anode temperature in the 23 °C environment, independent of the direction of the current flow. The increase in T_{anode} with discharge is counter to what the enthalpy model predicts: during discharge, the anode experiences a positive change in ΔS, therefore T_{anode} should decrease with discharge time.

While the enthalpy model (describing positive change in ΔS during discharge) may be correct, the data in Fig. 2A indicates the possibility of additional processes contributing to the state of T_{anode}. One such process is the resistive heating (i^2R_a) effected by the magnitude of the current (i) and the impedance of the anode (R_a); typically, R_a decreases with increase in temperature. At T_{env} = 23 °C (and at 0 °C, described in Section 3.3.1), the observation that $T_{anode} > T_{env}$ may be explained on the basis of the domination of i^2R_a-induced over the $T\Delta S$-related cooling. On the other hand, the observation that $T_{anode} < T_{env}$ when T_{env} = 38 or 45 °C (discussed in Section 3.3.2), may be explained if the entropy-induced cooling dominates over the i^2R_a. The competing aspects of $T\Delta S$ and i^2R_a at different T_{env} are discussed more quantitatively in Section 4.

3.2. Set 2, charging at 23 °C continuously after discharging

Fig. 3 shows the T_{env}, T_{surf} and T_{anode} data during the continuous charging after a discharge; the black line in the graph represents the discharge and charge currents (Y-axis on the right). The duration of the discharge portion shown in the figure is fairly short; nevertheless sufficient to elucidate the effect of the charging without resting. During charging, between 5% and 57% SoC, T_{surf} was slightly lower than the T_{env}. At the 57% SoC mark, the T_{surf} raised above T_{env} briefly, and stayed around T_{env} for the rest of the charging period. The initial drop in the T_{surf}, and the small increase around 57% SoC are consistent with the earlier observations by other research groups; however, the behavior is different from the data in Section 3.1, Fig. 2A. The T_{anode}, on the other hand, showed a continuous increase from the start of the charging, including the characteristic step-change in slope at 57% SoC, matching with the transition of the anode from Stage II (anode composition: LiC_{12}) to Stage I (anode composition: LiC_6). At all points along the line of charging, the T_{anode} remained constantly higher than the previous case (Fig. 2A), where the cell temperature was allowed to equilibrate with T_{env}. Throughout the course of charging, the higher temperature observed in Fig. 3 data as compared to those in Fig. 2A appears to have been caused by the residual heat that was present in the cell after the previous discharge, that was not allowed to dissipate before the recharge.

3.3. Set 3, high-rate discharge in 0, 23, 38 and 45 °C T_{env}

This set involves discharging the cell typically at rates >$C/5$ using a discharge profile: (−5 A ($C/10$) first 2 h; −25 A ($C/2$) for 24 min; −45 A ($C/1.11$) for 13 min; −10 A ($C/5$) for 1 h; and −5 A ($C/10$) until SoC reached 5%. The T_{anode} data obtained during the discharge at the four different temperatures (0, 23, 38 and 45 °C), along with the resistive impedance of the anode measured using impedance technique help explain further the entropy behavior of the anode.

3.3.1. Discharging using the multistep current profile in 0 °C and 23 °C T_{env}

The measured temperatures during the discharge in a 23 °C environment are shown in Fig. 4; in this figure, the color codes associated with the measured parameters are the same as in Fig. 3. For most of the discharge, the step changes in T_{surf} tracked well with the step changes in the discharge current: registering an increase of 0.25 °C during the $C/10$, 2 h discharge; about 1 °C during the $C/2$, 24-min discharge; about 3 °C during the $C/1.11$, 13-min discharge; about 1 °C during the $C/5$, 1-h discharge; and close to 23 °C during the $C/10$, final step of the discharge. The T_{anode} tracked the T_{surf} for most part of the discharge; at the highest rate of discharge ($C/1.11$), T_{anode} was higher than T_{surf} by up to 3 °C.

Fig. 5 shows the temperature versus time data during discharge at 0 °C. For most part, the T_{anode} and T_{surf} behavior in the 0 °C environment was similar to the behavior in the 23 °C environment. Only the magnitudes of the increase in temperature during step changes in the discharge current were higher for both T_{anode} and T_{surf}. Thus, in the 0 and 23 °C environment, the impact of discharge-induced positive change in ΔS in the anode, cooling and

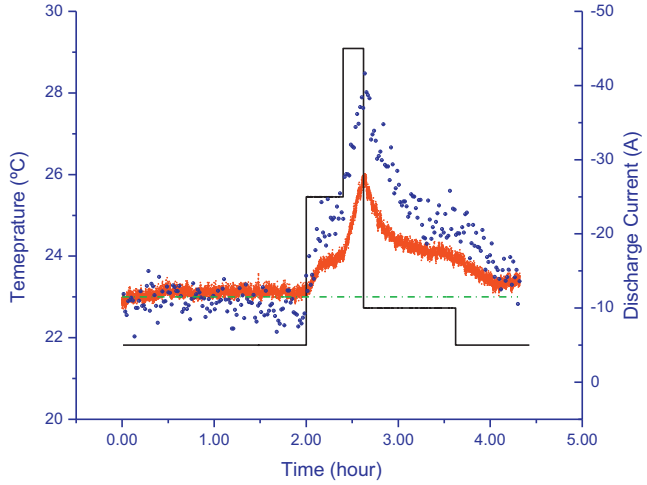

Fig. 4. Anode temperature, T_{anode} (blue), and surface temperature, T_{surf} (red) behavior of the cell in a 23 °C environment under discharge using a current profile as indicated by the solid black line and the Y-axis on the right. (For interpretation of the references to color in this figure legend, the reader is referred to the web version of the article.)

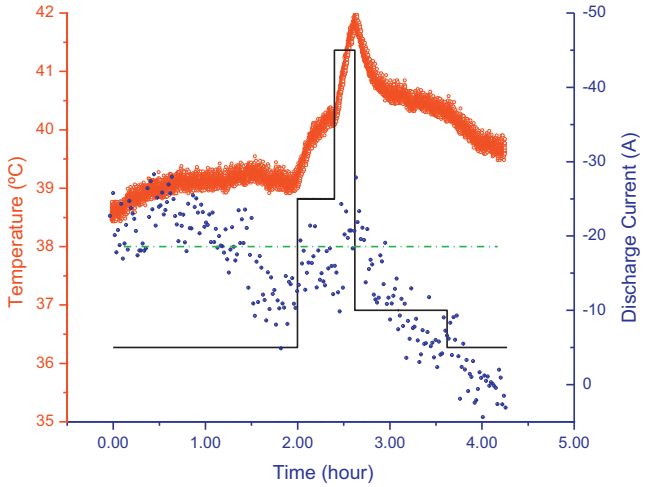

Fig. 6. Anode temperature, T_{anode} (blue), and surface temperature, T_{surf} (red) behavior of the cell in a 38 °C environment under discharge using a current profile as indicated by the solid black line and the Y-axis on the right. (For interpretation of the references to color in this figure legend, the reader is referred to the web version of the article.)

decreasing its temperature, was not found in the measured values of T_{anode}.

3.3.2. *Discharging using the multistep current profile 38 °C and 45 °C T_{env}*

Figs. 6 and 7 show the temperature versus time data during discharge in a 38 °C and 45 °C environment, respectively. The T_{anode} behavior is quite unlike that of the behavior at 0 and 23 °C. Although T_{surf} raised several degrees above the 38 °C (and 45 °C) environment, T_{anode} registered very little increase over the first hour of the $C/5$-rate discharge, and started dropping below the temperature of the environment after the first 1.5 h, when the SoC started falling below 70%. Except for small relative increases (<1 °C) during the $C/2$ and $C/1.1$ discharge steps, the slope of the T_{anode} versus time was always negative. If positive changes in ΔS during discharge is indeed capable of cooling the anode, it is clearly seen in the 38 °C and 45 °C environments.

The observed contrasting behavior of the anode during discharge: cooling when the cell is in the high-temperature (38 and 45 °C) environments, and heating when the cell is in the low-temperature (0 and 23 °C) environments, is indeed striking. The contrasting behavior is caused by the two competing phenomenon that contribute to the temperature of the anode under discharge: they are the entropy and resistive heating; more details are provided next in Section 4.

4. Resistive heating versus entropy for the carbon anode

The resistive impedance, R_a associated with the flow of lithium ions through the anode and the anode/electrolyte interface can generate heat during charging and discharging due to i^2R_a, where i is the amplitude of the current. In Li-ion cells, R_a is an experimentally measurable quantity, and is found to be dependent upon the temperature of the environment that the cell is in [8,10–12]. The dependence of R_a on T_{env} for the cell used in our tests (53-Ah GS

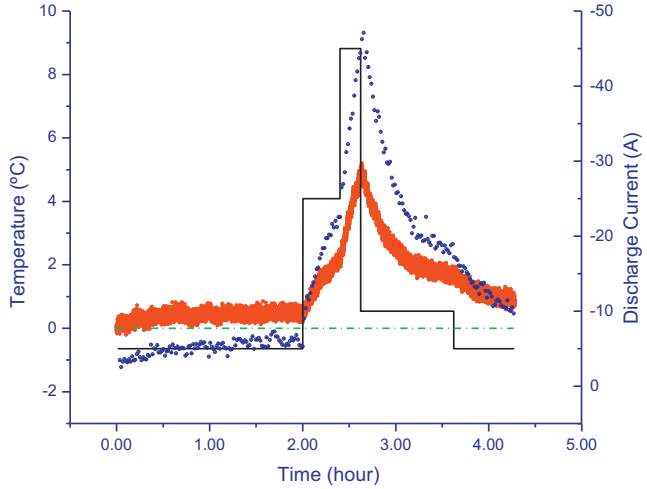

Fig. 5. Anode temperature, T_{anode} (blue), and surface temperature, T_{surf} (red) behavior of the cell in a 0 °C environment under discharge using a current profile as indicated by the solid black line and the Y-axis on the right. (For interpretation of the references to color in this figure legend, the reader is referred to the web version of the article.)

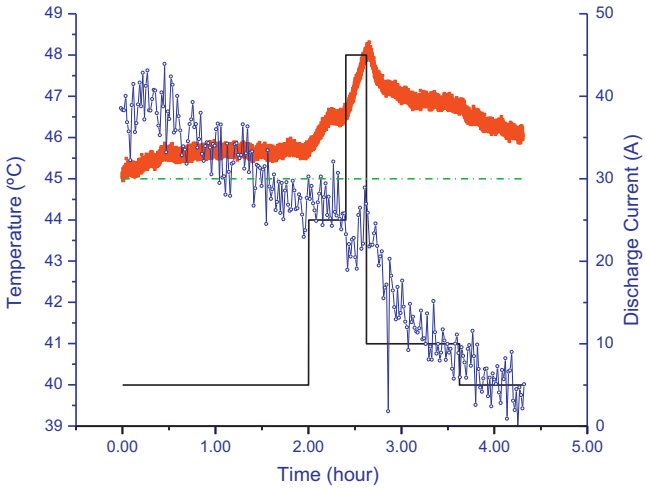

Fig. 7. Anode temperature, T_{anode} (blue), and surface temperature, T_{surf} (red) behavior of the cell in a 45 °C environment under discharge using a current profile as indicated by the solid black line and the Y-axis on the right. (For interpretation of the references to color in this figure legend, the reader is referred to the web version of the article.)

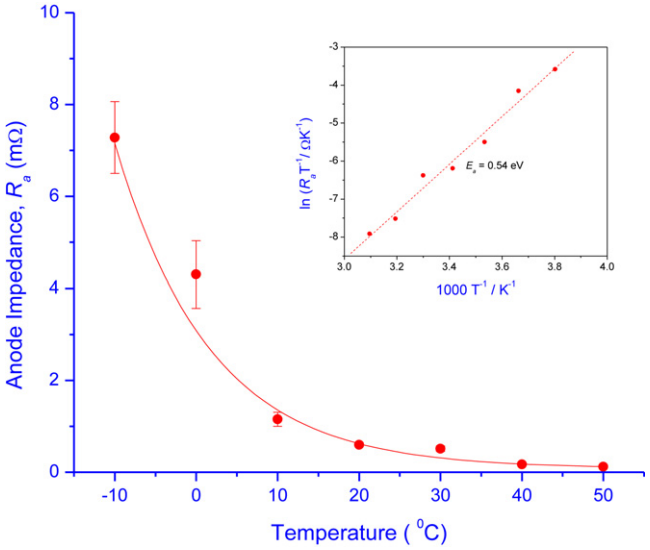

Fig. 8. Variation of the resistive impedance, R_a with the environmental temperature of the GS Yuasa cell. The red dots indicate experimental data obtained from impedance measurements. The solid line is a fit (exponential decay) to the experimental data. The inset shows the activation energy associated with R_a, estimated using Arrhenius equation, to be 0.54 eV. (For interpretation of the references to color in this figure legend, the reader is referred to the web version of the article.)

Yuasa) is shown in Fig. 8; the activation associated with R_a, estimated using Arrhenius equation, is indicated in the inset in the figure, and it is comparable to values reported earlier by us [8] and others [10]. At each temperature, the R_a and the error bars in the figure represent the average of measurements at nine different SoC values in the 10–90% range. Over the 0–45 °C range, the R_a dropped substantially, from 3.1-mΩ to 0.145-mΩ; the R_a vs. temperature data fitted to a single exponential decay, with a correlation coefficient of 0.943. The fitted data was used to interpolate R_a value at any temperature within the 0–45 °C range. Next, the i^2R_a values for different values of the discharge currents (5, 10, 25 and 45 A) were computed, and the results shown in Fig. 9A. Note that if i^2R_a were the only source of heat in an anode subject to discharge, then the anode would always register a higher temperature than that of the cell's environment, T_{env}. However, the data in Figs. 4 and 5 show that $T_{anode} > T_{env}$ only in the 0 and 23 °C environments and at discharge rates >C/10. In the 38 and 45 °C environments (Figs. 5 and 7), $T_{anode} < T_{env}$ virtually at all discharge rates, suggesting the dominance of yet another phenomenon, the positive change in ΔS in the anode that caused the anode to cool.

Entropy change, ΔS in the carbon anode is positive during discharge of Li-ion cells. The magnitude of ΔS is dependent on the lithium/carbon ratio, and the type of carbon used in preparing the anode [5,14,15,17]. For the purpose of comparing the ΔS-induced endothermic cooling with the exothermic resistive heating, we assume a ΔS of 8 J mol^{-1} K^{-1}. The equivalent lithium content in the 53-Ah cell is 15 g or 2.16 mol; assuming a 1.08 mol equivalence of lithium in a fully charged anode, the ΔS during full discharge (53-Ah) is 8 J mol^{-1} K^{-1} × 1.08 mol = 8.64 J K^{-1}. In the multistep discharge profile described in Section 3.3, the duration, τ', for the various discharge currents are 7200 s, 1440 s, 780 s and 3600 s, respectively for the −5-A, −25-A, −45-A and −10-A currents; within each step, the discharge capacity is 10-Ah that is equivalent to 18.9% of the full capacity, 53-Ah. In other words, for the 18.9% of 1.08 mol of the lithiated carbon, the associated change in entropy, $\Delta S' = 1.633$ J K^{-1}. The energy associated per second with the endothermic cooling is $T\Delta S'/\tau'$ in units of Watt (W). Thus, at 273 K, a 10-Ah discharge at −45 A rate would cause an endothermic cooling at the rate of −0.572 W; and only −0.062 W for the 10-Ah

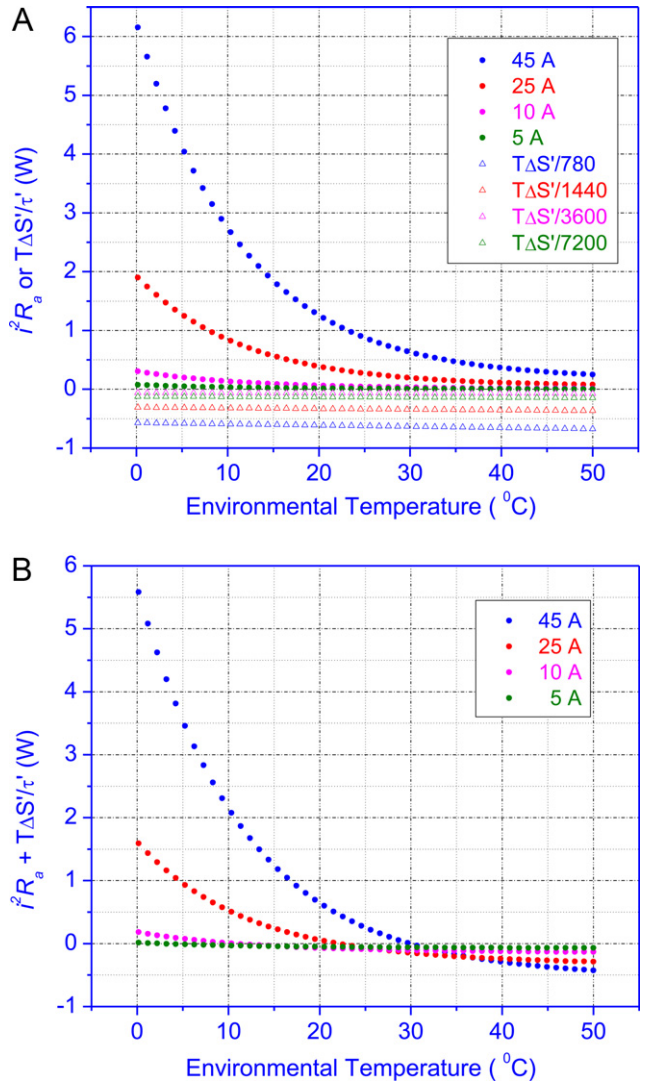

Fig. 9. Heating or cooling of the anode effected by entropy ($T\Delta S'/\tau'$) and resistive heating (i^2R_a) for the cell operating at different T_{env}: (A) the heat generated by i^2R_a, computed using the fitted data in Fig. 8 for i = 5, 10, 25 and 45 A. Also shown is the $T\Delta S'/\tau'$ dependence on T_{env} for $\Delta S' = 1.633$ J K^{-1} and $\tau' = 7200$ s, 3600 s, 1440 s and 780 s; and (B) the effect of T_{env} on the net ($i^2R_a + T\Delta S'/\tau'$) for the various currents.

discharge at −5 A rate. At 318 K and 10-Ah discharge, the rate of cooling would be −0.666 W at the −45 A rate and −0.072 W at the −5 A rate. Fig. 9A also shows entropy-associated cooling ($T\Delta S'/\tau'$) by discharging the cell to an equivalent of 10-Ah capacity at the rates of −45 A in 780 s, −25 A in 1440 s, −10 A in 3600 s and −5 A in 7200 s. Clearly, higher rates of discharge causes the more endothermic cooling. Next, we will examine the combined effect of $T\Delta S'/\tau'$ and i^2R_a.

If $\Delta S'$ was entirely responsible for determining the temperature of the anode, then during discharge, the anode temperature would always register a lower value than the temperature of the environment. However, when the resistive heating due to i^2R_a is taken into account, the net effect of ($i^2R_a + T\Delta S'/\tau'$) would influence the ($T_{anode} - T_{env}$) to transition from positive to negative; the transition temperature would depend upon T and τ'. The results of ($i^2R_a + T\Delta S'/\tau'$) shown in Fig. 9B indicate that: (i) while pulse discharging equivalent amounts of capacity (10-Ah) from a cell, the pulse with the most current in shortest time (45-A in 13 min) will influence the temperature of the cell most; and (ii) during low current discharge (rate <C/5) of the 53-Ah cell, the endothermic cooling due to $T\Delta S'/\tau'$ dominates over i^2R_a almost at all T_{env}. The

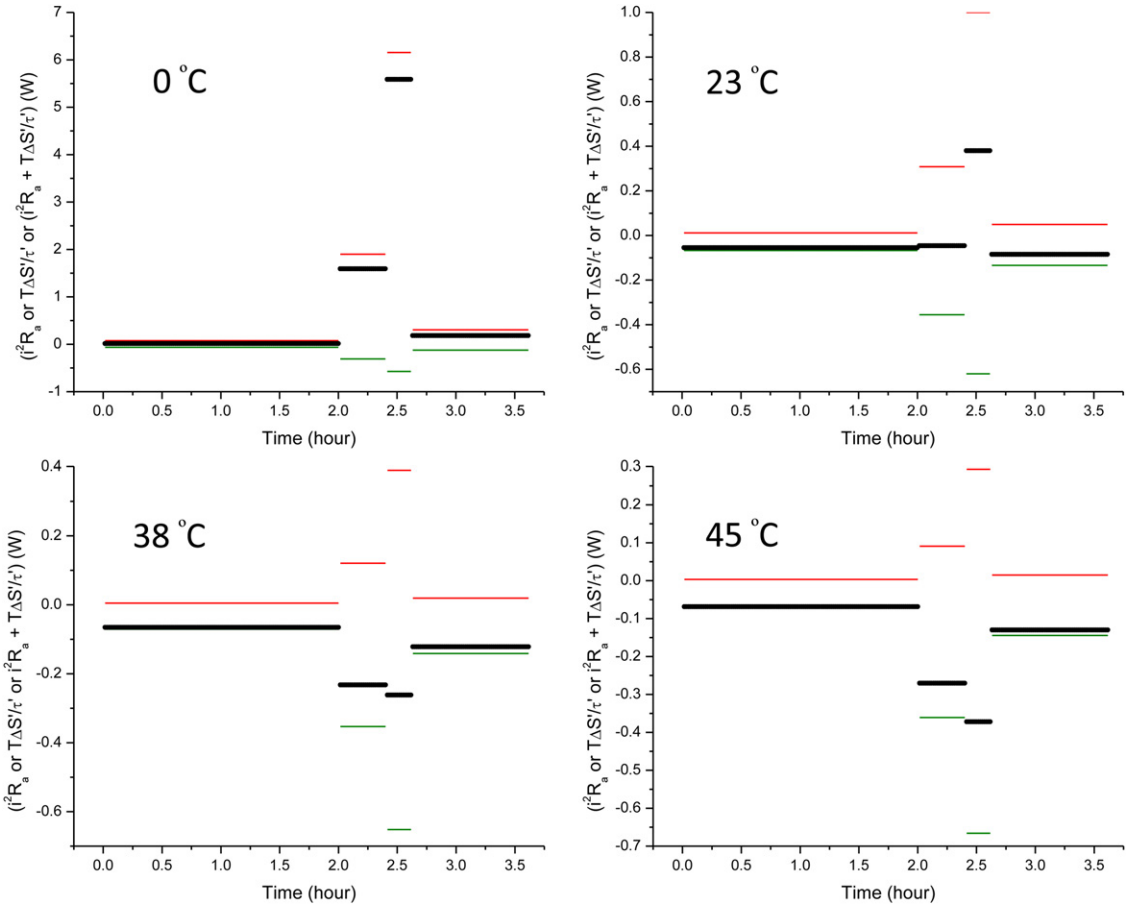

Fig. 10. Heating or cooling of the anode effected by entropy ($i^2R_a + T\Delta S'/\tau'$) at different T_{env} (0, 23, 38 and 45 °C) are shown in black. $\Delta S'$ corresponds to the discharge of 10-Ah capacity within a period of τ' that is 7200-s, 1440-s, 780-s and 3600-s, respectively at −5-A, −25-A, −45-A and −10-A discharge rates. The individual contributions of i^2R_a and $T\Delta S'/\tau'$ are represented by the red and olive green lines, respectively. (For interpretation of the references to color in this figure legend, the reader is referred to the web version of the article.)

calculated data in Fig. 9B is consistent with the experimental data in Figs. 2 and 4–7, where T_{anode} was always $<T_{env}$ only at low discharge rate (−5 A); and at high discharge rate (−45 A), T_{anode} was always $<T_{env}$ only at high T_{env} (>30 °C).

The net effect of the resistive heating and entropy-induced cooling, i.e. ($i^2R_a + T\Delta S'/\tau'$), viewed from the perspective of a pulse discharge similar to those in Figs. 4–7, is presented in Fig. 10. The figure represents entropy-induced cooling rate ($T\Delta S'/\tau'$) (in blue dotted line) for each 10-Ah segment of the discharge current profile in Figs. 4–7, the respective i^2R_a-induced heating (in red dotted line), and the net effect of ($i^2R_a + T\Delta S'/\tau'$) (in black) at 0, 23, 38 and 45 °C. The net effect ($i^2R_a + T\Delta S'/\tau'$) generates heating at all discharge rates only when T_{env} = 0 °C; at 38 and 45 °C, the net effect cools the anode, and in the intermediate 23 °C, the heating is pronounced when the discharge rate is at its highest (45-A). The resemblance of the power associated with ($i^2R_a + T\Delta S'/\tau'$) at the different T_{env} and the observed temperatures of the anode (Figs. 4–7) is quite striking.

The results of the thermodynamic model and its predictions in Figs. 9 and 10 are qualitatively in agreement with the experimental results in Figs. 4–7. Obviously, the exact T_{env} at which T_{anode} would transition from being relatively hot to cold in relationship to its environment depends upon the ΔS; the magnitude of ΔS depends upon the amount of lithium ion in the carbon anode as well as the type of carbon used in preparing the anode. A quantitative explanation will require an accurate estimate of ΔS of the anode of the 53-Ah GS Yuasa cell at different SoC, which is beyond the scope of the present work.

5. Conclusion

During discharge of a 53-Ah rechargeable Li-ion cell at >C/5 rates, the carbon anode heats up when the cell is operating at or below the normal room temperature, namely, 23 °C. When discharging at similar rates in an environment well above the normal room temperature such as 38 °C (100 F) or more, the anode cools down. During discharge, the anode is subject to both cooling and heating; the former by the positive changes in its entropy (ΔS), and the latter due to the resistive heating, i^2R_a associated with the flow of current, i across the impedance of the anode, R_a. Removal of lithium ions from the graphite during discharge [13], decreases the entropy of the graphite, leading to endothermic cooling [14,16,17]. The endothermic energy, $T\Delta S$ associated with entropy increases with T, therefore the anode cools more with increasing temperature of the environment, T_{env}. During pulse discharge, the magnitude of the pulse current (A) and its duration (τ') determines the total entropy change ($\Delta S'$) and the rate of endothermic cooling ($T\Delta S'/\tau'$) associated with the pulse.

The resistive heating, sometimes called the Joule heating, is associated with flow of an electric charge (current) through a resistance. Current flow through the anode during charge and discharge results in the addition or removal of the Li^+ through the SEI layer and the graphite lattice that offer the resistance, R_a. Since R_a is dependent on temperature [8–11], and decreases with increase in temperature, the i^2R_a has the opposite effect of the $T\Delta S'/\tau'$ during discharge: the energy associated with i^2R_a is smaller at higher

temperature and low rates of discharge. In practice, the endothermic cooling due to $T\Delta S'/\tau'$ exceeds the resistive heating due to i^2R_a when the cell is discharging at high rates ($\geq C/2$) in environments much higher than the room temperature; at or below the room temperature, $T\Delta S'/\tau'$ is too small to compensate for i^2R_a, allowing the anode to heat up.

Traditionally, it has been possible to measure the heat associated with the lithiation and de-lithiation processes in of carbon anodes (equivalent to charging and discharging of a Li-ion cell), only using carbon half-cells and calorimeters [14,16]; techniques involving temperature sensors inserted inside the cell provides an average value of the anode/separator, electrolyte/cathode ensemble [18]. A new electrical four-probe technique recently developed by us [8,9], has enabled to measure the temperature of the anode, T_{anode} in a Li-ion cell under charge or discharge. The technique known as Battery Internal Temperature Sensor (BITS), is based on the measurement of phase shift (ϕ) between the current and voltage of a low-amplitude 40-Hz sinusoidal signal applied across the positive and negative terminals of the cell. The technique is useful in monitoring the T_{anode} on-line, while the cell is subject to charge and discharge.

BITS also helped to identify that charging a cell at manufacturer-recommended rates of $C/5$ in a 23 °C environment heats up the anode, even though the cell as a whole experiences cooling as evidenced by the temperature recorded at the cell's external surface (T_{surf}) [19]. Decrease in T_{surf}, and increase in T_{anode} during charging are both consistent with the prediction made by earlier thermodynamic models of and measured entropy changes in carbon anodes and Li-ion cells [5,14–17,19]. The extent of decrease in T_{surf}, and increase in T_{anode} are, however, dependent on if the charging happened immediately after discharging, or the cell was allowed to equilibrate with the environment prior to charging.

Acknowledgements

Financial assistance for this study was provided by the Independent Research and Development Program, National Security Space Business Area, Applied Physics Laboratory (APL), Johns Hopkins University. The author would like to thank Richard Fitzgerald, Radiation Belt Storm Probes Project Manager at APL, for his support. In addition, the author would like to thank Carson Baisden, Michael Butler and Bliss Carkhuff of the APL for valuable discussions.

References

[1] Z. Chen, Y. Qin, J. Liu, K. Amine, Electrochem. Solid State Lett. 12 (2009) A69–A72.
[2] I.A. Profatilova, S.S. Kim, N.-A. Choi, Electrochim. Acta 54 (2009) 4445–4450.
[3] S. Shriram, R. Premanand, Z. John (Zhengming), J. Power Sources 194 (2009) 550–557.
[4] Jeff VanZwol, Power Electronics Technology, 2006 July, pp. 40–45 (www.powerelectronics.com).
[5] R.E. Williford, V.V. Viswanathan, J.-G. Zhang, J. Power Sources 189 (2009) 101–107.
[6] P.G. Balakrishnan, R. Ramesh, T. Prem Kumar, J. Power Sources 155 (2006) 401–414.
[7] A.M. Andersson, M. Herstedt, A.G. Bishop, K. Edström, Electrochim. Acta 47 (2002) 1885–1898.
[8] R. Srinivasan, B.G. Carkhuff, M.E. Butler, A.C. Baisden, Electrochim. Acta 56 (2011) 6198–6204.
[9] R. Srinivasan, B.G. Carkhuff, M.H. Butler, A.C. Baisden, O.M. Uy, Proceedings of the SPIE conference on Defense, Security and Sensing, 25–29 April 2011, Orlando, FL, USA, 2011, Paper No. 8035-13.
[10] P. Suresh, A.K. Shukla, N. Munichandraiah, J. Appl. Electrochem. 32 (2002) 267–273.
[11] S.S. Zhang, K. Xu, T.R. Jow, Electrochim. Acta 49 (2004) 1057–1061.
[12] G. Nagasubramanian, J. Appl. Electrochem. 31 (2001) 99–104.
[13] M. Winter, K.-C. Moeller, J.O. Besenhard, in: G.-A. Nazri, G. Pistoia (Eds.), Lithium Batteries: Science and Technology, Kluwer Academic Publishers, NY, 2004, p. 153.
[14] Y. Reynier, R. Yazami, B. Fultz, J. Power Sources 119–121 (2003) 850–855.
[15] H. Vaidyanathan, W.H. Kelly, G. Rao, J. Power Sources 93 (2001) 112–122.
[16] Y. Reynier, R. Yazami, B. Fultz, I. Barsukov, J. Power Sources 165 (2007) 552–558.
[17] Q. Huang, M. Yan, Z. Jiang, J. Power Sources 156 (2006) 541–546.
[18] C. Forgez, D.V. Do, G. Friedrich, M. Morcrette, C. Delacourt, J. Power Sources 195 (2010) 2961–2968.
[19] V.V. Viswanathan, D. Choi, D. Wang, W. Xu, S. Towne, R.E. Williford, J.-G. Zhang, J. Liu, Z. Yang, J. Power Sources 195 (2010) 3720–3729.